Repeating earthquakes and seismic potential along the northern Longitudinal Valley fault of eastern Taiwan

Ruey-Juin Rau,[1] Kate Huihsuan Chen,[1] and Kuo-En Ching[1]

Received 9 August 2007; revised 5 November 2007; accepted 12 November 2007; published 18 December 2007.

[1] The northern Longitudinal Valley fault in eastern Taiwan creeps at the surface with a small rate of ~1 cm/yr but slips in large earthquakes. To improve seismic hazard assessment, it is important to comprehend the slip deficit rate distribution at depth. We discovered 25 M_L 2.1–4.6 repeating earthquakes in this area and inverted GPS measurements for producing an image of the along-strike spatial distribution of deep fault slip rates. The repeating events are located at the depths of 10–22 km with 24.9–77.5 mm/yr slip rates, which are comparable with the GPS-derived slip rates of 47.5 ± 5.8 mm/yr at similar depth ranges. Based on distribution of GPS-derived slip deficits, since 1951, the northern Longitudinal Valley fault has become capable of releasing stored strain in a future M_w = 7.3 earthquake. **Citation:** Rau, R.-J., K. H. Chen, and K.-E. Ching (2007), Repeating earthquakes and seismic potential along the northern Longitudinal Valley fault of eastern Taiwan, *Geophys. Res. Lett.*, *34*, L24301, doi:10.1029/2007GL031622.

1. Introduction

[2] There is now ample evidence that observations of repeating earthquakes (i.e., a group of earthquakes that repeatedly rupture at the same fault patch with highly similar waveforms, locations, sizes, and focal mechanisms) indicate an aseismic slip of a creeping fault zone. First, repeating earthquakes have been found along well recognized creeping faults and are located away from locked zones [e.g., *Ellsworth and Dietz*, 1990; *Vidale et al.*, 1994; *Nadeau et al.*, 1995; *Rubin et al.*, 1999; *Matsuzawa et al.*, 2002; *Nadeau and McEvilly*, 2004]. Second, the deep slip rates derived from the repeating earthquakes are strongly correlated to the surface rate suggesting unimpeded creeping from the surface to the depths where repeating events are located [*Nadeau and McEvilly*, 1999; *Bürgmann et al.*, 2000]. Third, numerical, analytic and laboratory experiments have been conducted to understand the mechanics of these repeating microearthquakes [e.g., *Anooshehpoor and Brune*, 2001; *Beeler et al.*, 2001; *Sammis and Rice*, 2001; *Johnson and Nadeau*, 2002], which suggest that the repeatedly ruptured asperities are likely surrounded by stable-sliding material where significant aseismic slip is taking place. Seismically active regions with numerous repeating events, therefore, indicate aseismic slip at depth.

[3] Given an assumption that the frequency of seismic slips on an asperity is proportional to the tectonic loading rate of the relative plate motion, one can determine the deep fault slip rate at each repeating sequence site using the relationship between the recurrence intervals and seismic moments of repeating sequence [*Nadeau and Johnson*, 1998; *Nadeau and McEvilly*, 1999, 2004]. Therefore, in the regions where the deep fault behavior is not known due to the poor and/or sparse coverage of geodetic and seismic stations, repeating earthquake observations, if any, is valuable for studying creep rate at depth.

[4] Our study area is located at the creeping Longitudinal Valley fault (LVF) in eastern Taiwan (Figure 1a). The fault to the south slips through creep and small earthquakes, and to the north which was ruptured by several M = 7 earthquakes in 1951. With one-sided station coverage (Figure 1a), an understanding of deep fault behavior along the LVF has been limited. The fault slip rate at depth in the southern segment of the LVF is presented using repeating earthquakes (K. H. Chen et al., Characteristic repeating earthquakes in an arc-continent collision boundary zone: The Chihshang fault of eastern Taiwan, submitted to *Earth and Planetary Science Letters*, 2007, hereinafter referred to as Chen et al., submitted manuscript, 2007), whereas in the north, deep fault deformation as well as its implication to earthquake hazard is still not known. In this paper we searched for repeating earthquakes along the northern LVF zone and calculated the deep fault slip rates from repeating earthquake sequences. We then inverted surface GPS velocities for fault slip deficit rates and, together with the deep fault slip rate derived from repeating earthquake sequences, we discussed their implications to earthquake potential along the northern LVF.

2. Northern Longitudinal Valley Fault of Eastern Taiwan

[5] The interaction between two subduction systems of opposite polarity is taking place near Taiwan: the Philippine Sea plate subducts beneath the Eurasian plate to the northeast, whereas the Eurasian plate goes underneath the Philippine Sea plate to the south. Between these two plates, the convergence rate is 7–8 cm/yr [*Seno*, 1977; *Yu et al.*, 1997]. The LVF is a 160-km long and NNE-striking distinct morphological feature and marks the boundary between the two plates in eastern Taiwan (Figure 1a). Due to a reversal of the subduction direction, the LVF dips eastward in the south with reverse motion, whereas in the north it dips northwestward or westward with also a dominant reverse component [e.g., *Chemenda et al.*, 1997; *Kao and Jian*, 2001; *Kim et al.*, 2006]. The southern portion of the LVF is characterized by a creeping behavior with slip rate of 2–3 cm/yr at surface [*Liu and Yu*, 1990; *Angelier et al.*, 2000] and 2–5 cm/yr at 10–20 km depth [*Hsu et al.*, 2003; *Johnson et al.*, 2005] where the major fault segment, the

[1]Department of Earth Sciences, National Cheng Kung University, Tainan, Taiwan.

0094-8276/07/2007GL031622$05.00

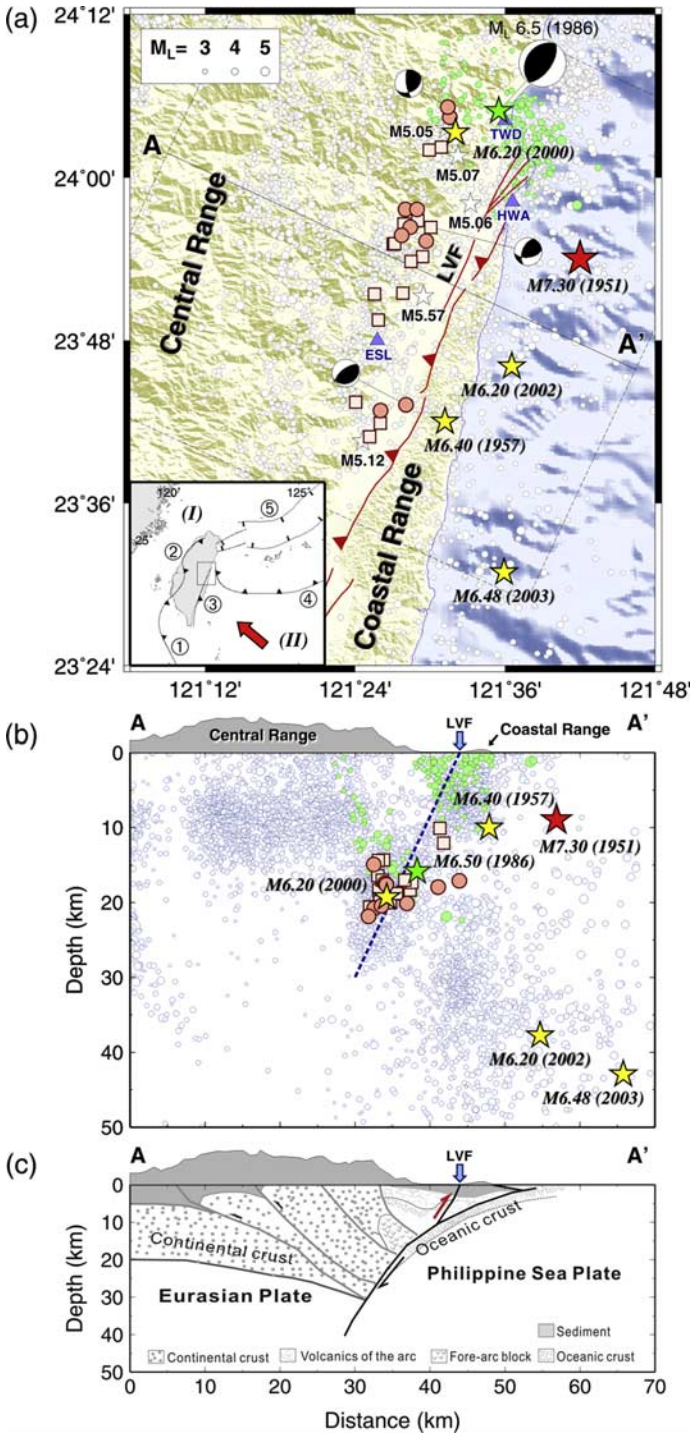

Figure 1. (a) Location of the northern LVF in eastern Taiwan. Inset shows the plate tectonics of Taiwan and the study area in the box. Numerals, 1–5, are the Manila trench, the deformation front, the LVF, the Ryukyu trench, and the Okinawa trough, respectively. $M \geq 3$ seismicity relocated by HypoDD [*Waldhauser and Ellsworth*, 2000] during 1991–2004 is shown in white circles. Green circles are locations of the aftershock distribution of the 1986 M 6.5 event. Locations of the 9 repeating sequences used to estimate fault slip rate are shown as red circles while other 16 repeating sequences are shown as squares. White stars are M 5–6 earthquakes and yellow stars are $M \geq 6$ earthquakes that occurred in the study region. Seismic stations are shown as blue triangles. (b) Locations of background seismicity (white circles), large events (stars), and repeating sequences (red circles and squares) along the fault-perpendicular profile A-A′. Blue dash line denotes the location of modeled fault plane. Aftershock distribution of the 1986 M 6.5 earthquake, shown in green circles, presents two prominent clusters. The first one appears as a high-angle east-dipping zone to the west under the Central Range and the aftershocks in the second cluster spread diffusely to the east beneath the northern LVF. The hypocenter of the 1986 M 6.5 mainshock is located at the intersection of these two clusters. (c) Schematic crustal model of cross section (A-A′) modified from *Chemenda et al.* [2001].

Chihshang fault, exhibits a contrasting deep fault slip behavior of creeping to the north and locked to the south using repeating earthquake observations (Chen et al., submitted manuscript, 2007). The northern portion of the LVF has a smaller surface slip rate of ~1 cm/yr [*Yu and Kuo*, 2001] (Figure 2), but with a high slip rate (5–6 cm/yr) at depth [*Hsu et al.*, 2003; *Johnson et al.*, 2005]. Thus the northern segment of the LVF is likely characterized by higher probabilities for a large earthquake.

3. Repeating Earthquakes Search

[6] To search for repeating earthquakes in the northern LVF zone, we used waveform data of 5613 earthquakes recorded by the Central Weather Bureau Seismic Network (CWBSN) during the period 1991–2004 within a grid between 23.4 and 24.2°N, 121.2 and 121.6°E. Figure 1 shows seismicity in the study period in mapview and cross section, respectively, together with schematic crustal model of the cross section across the northern LVF. The seismograms were re-sampled at 1000 samples per second in order to obtain the sub-sample precision, and then bandpass filtered from 2 to 18 Hz. Maximum cross-correlation coefficients (ccc) between all seismogram pairs were determined using a 10.5 second window beginning 0.5 second before the P-arrival. For this study, we used vertical component seismograms from 7 to 10 CWBSN stations having relatively low noise level (station locations and waveform examples are shown in Figures S1 and S2 of the auxiliary materials, respectively). Among these stations, only ESL, HWA, and TWD are local to the study area, as shown in Figure 1. Here we use a composite selection criteria that incorporates both waveform similarity (wfs) and differential S-P (dSmP) time information and allows exclusion of outliers in the wfs and dSmP data to identify repeating earthquakes (Chen et al., submitted manuscript, 2007). A description of the method of composite selection criteria and its agreement with earthquake relocation result is shown in Figures S3 and S4 in the auxiliary material.

4. Repeating Sequences Distribution

[7] Using the composite selection criteria, we identified 25 repeating sequences in the northern LVF zone containing 95 repeating events with magnitudes of 2.1 to 4.6. The number of events in a repeating sequence ranges from 3 to 6 (see event chronologies in Figure S5 in the auxiliary materials). This represents about 1.6% of all the earthquakes in the starting catalog. Locations of the 25 repeating sequences with depths of 10–22 km are shown by the red circles in Figure 1.

[8] The along-strike variation in deep creep rates can be revealed using the relationship between the recurrence intervals and seismic moments of repeating sequence events [*Nadeau and Johnson*, 1998; *Nadeau and McEvilly*, 1999, 2004; *Matsuzawa et al.*, 2002; *Igarashi et al.*, 2003; *Uchida et al.*, 2003]. The method first relates the seismic moment of a repeated event (*Mo*) to the surrounding aseismic fault slip (d_i) that loads the event's rupture patch to failure during its preceding recurrence interval.

$$d_i = 10^{\alpha} M_0^{\beta}, \quad (1)$$

where $\alpha = -2.36 \pm 0.16$ and $\beta = 0.17 \pm 0.01$, which were empirically derived from earthquake and geodetic data at Parkfield, California [*Nadeau and Johnson*, 1998], and have also been used to infer deep slip rates in other regions outside Parkfield (e.g., along the Japan subduction zone [*Matsuzawa et al.*, 2002; *Igarashi et al.*, 2003; *Uchida et al.*, 2003]). Using the above slip measurements and the corresponding event epoch, we solved for the best-fit slip rate in a least-squares sense. Our error analysis shows that the uncertainty in slip rate estimate increases with the lifetime (i.e., duration) of the repeating sequence, where a clear break in the statistics can be seen at 6 years duration (see Figure S6 in the auxiliary material).[1] We therefore chose the repeating sequences with duration longer than 6 years to determine their slip rates (denoted by colored circles in Figure 3). The derived slip rates range 24.9–77.5 mm/yr and the average slip rate is 55.1 mm/yr with 1-sigma of 17.5 mm/yr (Figure 3).

5. Slip Deficit Along the Northern LVF

[9] Although the interseismic slip rates at depth can be directly determined from the repeating earthquake sequences, asperities defined by slip deficit rate distribution on the northern LVF remains to be determined. We therefore inferred the slip deficit rates (i.e., back-slip rates) and block velocities on the northern LVF by modeling the horizontal GPS observations [*Yu and Kuo*, 2001] (Figure 2) using the 3D block model in an elastic, homogenous and isotropic half space. The deep slip rates (sum of slip deficit rate and block velocity [*Savage*, 1983; *Matsu'ura et al.*, 1986]) resulted from block modeling are also compared with the slip rates derived from repeating earthquake sequences to examine their consistencies.

[10] The location, strike, and fault length (77 km) of the modeled plane are deduced from the tomographic study of eastern Taiwan [*Kim et al.*, 2006] (Figure 2). Fault dip angle of 65° and depth of the fault bottom (30 km) are chosen according to the seismicity distribution (Figure 1b) and the inferred dip angles of composite focal mechanisms of three $M_L \geq 3.8$ repeating earthquakes (Figure 1a). The fault plane is divided into 20 × 10 patches. The Green's function **G**, derived from the analytic expressions of *Okada* [1985], determines surface velocity components due to slip along the fault patches. The slip parameter vector **s** consists of the back-slip rate for each fault patch and the block velocity. Horizontal GPS velocities are described in data vector **d**. The relationship between data vector and the slip parameter vector is expressed by $\mathbf{As} = \mathbf{d}$. Here **A** comprises **G** and $\mathbf{G_b}$, where $\mathbf{G_b}$ is the function related to the surface velocity and block motion. The reciprocal of uncertainty of velocities is adopted as the weighting factor. Then we minimized the following function to yield the best estimate,

$$F(\mathbf{s}, \beta) = \left|\left| \sum^{-1/2} (\mathbf{As} - \mathbf{d}) \right|\right|^2 + \beta^{-2} ||\nabla^2 \mathbf{s}||^2, \quad (2)$$

where ∇^2 is a finite-difference Laplacian operator and β is a smoothing parameter. The agreement of model predictions

[1] Auxiliary materials are available in the HTML. doi:10.1029/2007GL031622.

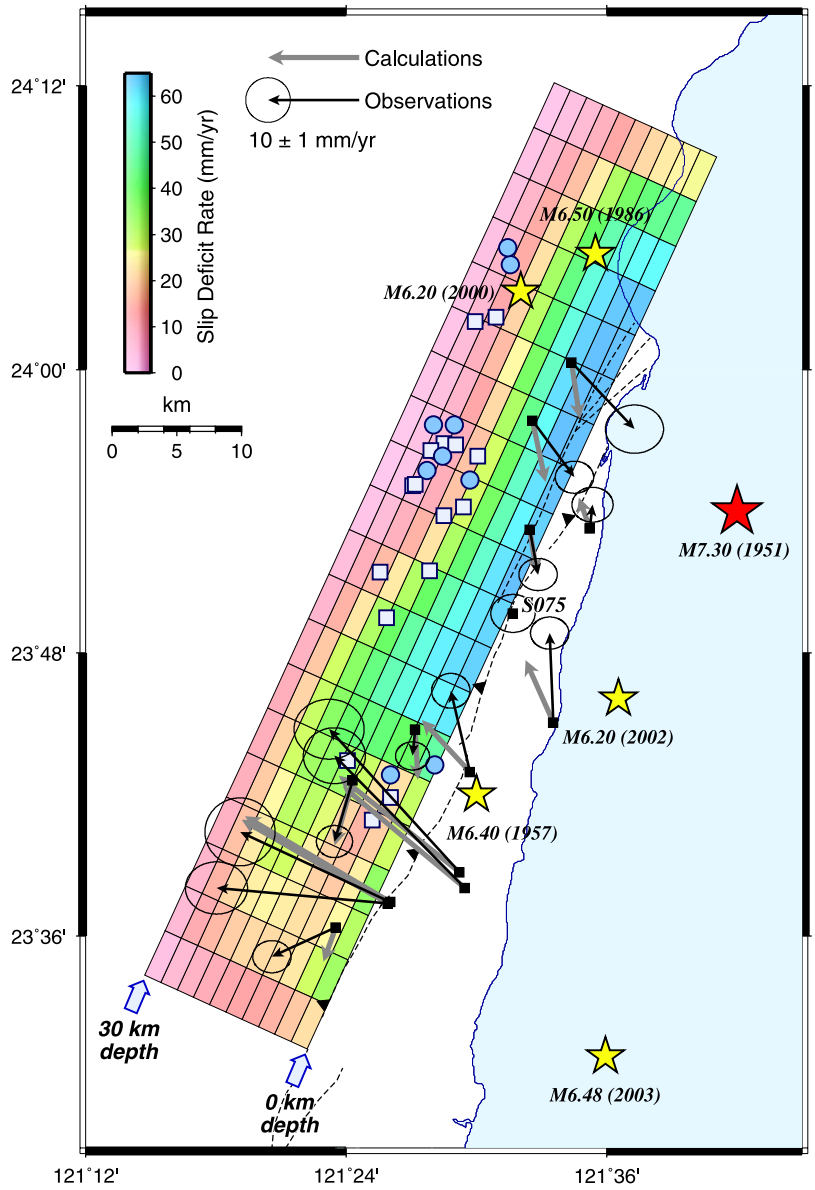

Figure 2. Inferred slip deficit rates on the northern LVF. Depths of modeled fault top and bottom are shown at the southernmost bound of the projected fault plane. Black vectors indicate GPS velocities (1992–1999, *Yu and Kuo* [2001]) relative to the station S075 on the eastern side of the LVF. Grey vectors are calculated velocities. Blue circles and light blue squares, as explained in Figure 1, are locations of repeating sequences.

and data is evaluated by the weighted residual sum of squares $WRSS = (\mathbf{d_{obs}} - \mathbf{d_{cal}})^{T} \cdot \mathbf{cov}^{-1} \cdot (\mathbf{d_{obs}} - \mathbf{d_{cal}})$, where $\mathbf{d_{obs}}$ and $\mathbf{d_{cal}}$ are the observations and calculations, respectively, and cov is the data covariance matrix.

[11] The WRSS of the optimized model is 15.2 mm/yr with the chosen smoothing parameter as 0.8 (trade-off pattern of WRSS and smoothing factors is shown in Figure S7 of the auxiliary materials). The best-fit block motion on the hanging wall (eastern block) of the LVF is 40.1 mm/yr toward 167.5°, which corresponds to the long-term slip rate of 65.5 mm/yr with rake of 60.7° on the fault plane, relative to the footwall. This long-term slip rate is consistent with the previous inferred slip rate (5–6 cm/yr) on the northern portion of the LVF [*Hsu et al.*, 2003; *Johnson et al.*, 2005]. The distribution of backward strike-slip and dip-slip components and the coupling ratio distribution along the fault plane are represented in Figure S8 in the auxiliary material. The slip deficit rate distribution and the calculated velocities are represented in Figure 2. Dominant locking fault patches are mainly located in the shallow part (0–18 km depth) of the northern fault segment between 8 and 54 km from the northernmost tip of the fault trace. Assuming the shear modulus as 3.3×10^{10} N/m^2, the moment deficit rate is 2.43×10^{18} N-m/yr. The interseismic slip rate shown in Figure 3 is the difference between the long-term slip rate and slip deficit rate. To compare with the repeater-derived slip rate, we calculated the average GPS-derived slip rates between 15 and 25 km depth of 20 fault segments along the fault strike (Figure 3). The result indicates that the GPS-derived slip rate of 47.5 ± 5.8 mm/yr is comparable with the repeater-derived slip rate of 55.1 ± 17.5 mm/yr.

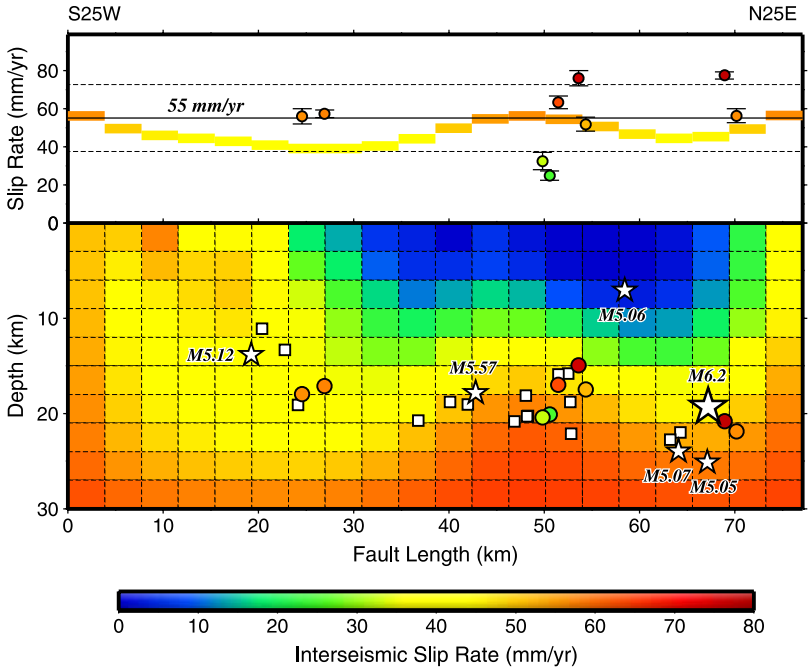

Figure 3. (bottom) Spatial distribution of inferred interseismic slip rates and repeating sequence along the northern LVF. Colored circles and white squares, as explained in Figure 1, represent locations of repeating sequences. Colors are keyed to the slip rates. White stars indicate major events occurring during 1991–2004. (top) Colored circles show a projection of repeaters with their corresponding slip rates on the along-strike distance, solid black line denotes the average slip rate from repeaters and 1-sigma standard deviation is shown as dashed lines. Colored lines are the average GPS-derived slip rates between 15 and 25 km depth of 20 fault segments along the fault strike.

[12] During the last century, the 1951 M_L = 7.3 Hualien-Taitung earthquake (Figure 1) ruptured the LVF from north to south in a time span of ~1 month [*Cheng et al.*, 1996; *Chen et al.*, 2007]. We suggested that the 1951 earthquake sequence had likely released the entire seismic moment stored in the fault zone. Then the derived moment deficit rate on the northern LVF leads to an accumulated moment deficit of 1.34×10^{20} N-m over 55 years from 1951 to 2006. In the same time period, only three large earthquakes occurred in the northern LVF zone (Figure 1a). They are the 1957 M_L = 6.4 event, the 1986 M_L = 6.5 event, and the 2000 M_L = 6.2 event, respectively. The seismic moment summation of all these three events is 5.64×10^{18} N-m, which only takes up 4.2% of the total deficit accumulation since the 1951 events. The stored moment deficit from 1951 to 2006 is therefore calculated to be 1.28×10^{20} N-m, corresponding to an M_w = 7.3 earthquake.

6. Conclusions

[13] We reported on 25 M_L = 2.1–4.6 repeating earthquake sequences with focal depths of 10–22 km occurred in the northern LVF area during the 1991–2004 study period. From these repeating earthquakes, we estimated their average deep slip rate to be 24.9–77.5 mm/yr. These observations suggest that localized deep slip is occurring on the northern LVF. On the other hand, the slip deficit and block velocity estimates from GPS observations suggest that the 47.5 ± 5.8 mm/yr interseismic slip rate in depth ranges of 15–25 km is comparable with those inferred from the repeating earthquake sequences. The optimal block model of northern LVF indicates that the stored slip deficit is equivalent to a 1.28×10^{20} N-m moment deficit from 1951 to 2006, which corresponds to an M_w = 7.3 earthquake.

[14] **Acknowledgments.** The manuscript benefited from critical comments from two anonymous reviewers. This research was partially supported by Taiwan NSC grant 96-2116-M-006-011. This is Taiwan Earthquake Research Center contribution 19.

References

Angelier, J., H. T. Chu, J. C. Lee, and J. C. Hu (2000), Active faulting and earthquake hazard: The case study of the Chihshang Fault, Taiwan, *J. Geodyn.*, *29*, 151–185.

Anooshehpoor, A., and J. N. Brune (2001), Quasi-static slip rate shielding by locked and creeping zones as an explanation for small repeating earthquakes at Parkfield, *Bull. Seismol. Soc. Am.*, *91*(2), 401–403.

Beeler, N. M., D. L. Lockner, and S. H. Hickman (2001), A simple stick-slip model for repeating earthquakes and its implication for microearthquakes at Parkfield, *Bull. Seismol. Soc. Am.*, *91*(6), 1797–1804.

Bürgmann, R., D. Schmidt, R. M. Nadeau, M. d'Alessio, E. Fielding, D. Manaker, T. V. McEvilly, and M. H. Murray (2000), Earthquake potential along the Northern Hayward Fault, California, *Science*, *289*, 1178–1182.

Chemenda, A. I., R. K. Yang, C. H. Hsieh, and A. L. Groholsky (1997), Evolutionary model for the Taiwan collision based on physical modeling, *Tectonophysics*, *274*, 253–274.

Chemenda, A. I., R. K. Yang, J. F. Stephan, E. A. Konstantinovskaya, and G. M. Ivanov (2001), New results from physical modelling of arc-continent collision in Taiwan: Evolutionary model, *Tectonophysics*, *333*, 159–178.

Chen, K. H., S. Toda, and R.-J. Rau (2007), A leaping, triggered sequence along a segmented fault: The 1951 ML 7.3 Hualien-Taitung earthquake sequence in eastern Taiwan, *J. Geophys. Res.*, doi:10.1029/2007JB005048, in press.

Cheng, S. N., Y. T. Yeh, and M. S. Yu (1996), The 1951 Taitung earthquake in Taiwan, *J. Geol. Soc. China*, *39*, 267–285.

Ellsworth, W. L., and L. D. Dietz (1990), Repeating earthquakes: Characteristics and implications, in *Proceedings of Workshop XLVI, the 7th U.S.–Japan Seminar on Earthquake Prediction*, *U.S. Geol. Surv. Open File Rep.*, *90–98*, 226–245.

Hsu, Y.-J., M. Simons, S.-B. Yu, L.-C. Kuo, and H.-Y. Chen (2003), A two-dimensional dislocation model for interseismic deformation of the Taiwan mountain belt, *Earth Planet. Sci. Lett.*, *211*, 287–294.

Igarashi, T., T. Matsuzawa, and A. Hasegawa (2003), Repeating earthquakes and interplate aseismic slip in the northeastern Japan subduction zone, *J. Geophys. Res.*, *180*(B5), 2249, doi:10.1029/2002JB001920.

Johnson, K. M., P. Segall, and S. B. Yu (2005), A viscoelastic earthquake cycle model for Taiwan, *J. Geophys. Res.*, *110*, B10404, doi:10.1029/2004JB003516.

Johnson, P. A., and R. M. Nadeau (2002), Asperity model of an earthquake: Static problem, *Bull. Seismol. Soc. Am.*, *92*(2), 672–686.

Kao, H., and P. R. Jian (2001), Seismogenic patterns in the Taiwan region: Insights from source parameter inversion of BATS data, *Tectonophysics*, *333*, 179–198.

Kim, K. H., J. M. Chiu, J. Pujol, and K. C. Chen (2006), Polarity reversal of active plate boundary and elevated oceanic upper mantle beneath the collision suture in central eastern Taiwan, *Bull. Seismol. Soc. Am.*, *96*(3), 796–806.

Liu, C. C., and S. B. Yu (1990), Vertical crustal deformations in eastern Taiwan and its tectonic implications, *Tectonophysics*, *183*, 111–119.

Matsu'ura, M., D. D. Jackson, and A. Cheng (1986), Dislocation model for aseismic crustal deformation at Hollister, California, *J. Geophys. Res.*, *91*, 12,661–12,674.

Matsuzawa, T., T. Igarashi, and A. Hasegawa (2002), Characteristic small-earthquake sequence off Sanriku, northern Honshu, Japan, *Geophys. Res. Lett.*, *29*(11), 1543, doi:10.1029/2001GL014632.

Nadeau, R. M., and L. R. Johnson (1998), Seismological studies at Parkfield VI: Moment release rates and estimates of source parameters for small repeating earthquake, *Bull. Seismol. Soc. Am.*, *88*(3), 790–814.

Nadeau, R. M., and T. V. McEvilly (1999), Fault slip rates at depth from recurrence intervals of repeating microearthquakes, *Science*, *285*, 718–721.

Nadeau, R. M., and T. V. McEvilly (2004), Periodic pulsing of characteristic microearthquakes on the San Andreas fault, *Science*, *303*, 220–222.

Nadeau, R. M., W. Foxall, and T. V. McEvilly (1995), Clustering and periodic recurrence of microearthquakes on the San Andreas fault at Parkfield, California, *Science*, *267*, 503–507.

Okada, Y. (1985), Surface deformation due to shear and tensile faults in a half space, *Bull. Seismol. Soc. Am.*, *75*, 1135–1154.

Rubin, A. M., D. Gillard, and J. L. Got (1999), Streaks of microearthquakes along creeping faults, *Nature*, *400*, 635–641.

Sammis, C. G., and J. R. Rice (2001), Repeating earthquakes as low-stress-drop events at a border between locked and creeping fault patches, *Bull. Seismol. Soc. Am.*, *91*(3), 532–537.

Savage, J. C. (1983), A dislocation model of strain accumulation and release at a subduction zone, *J. Geophys. Res.*, *88*, 4984–4996.

Seno, T. (1977), The instantaneous rotation vector of the Philippine Sea plate relative to the Eurasian plate, *Tectonophysics*, *42*, 209–226.

Uchida, N., T. Matsuzawa, A. Hasegawa, and T. Igarashi (2003), Interplate quasi-static slip off Sanriku, NE Japan, estimated from repeating earthquakes, *Geophys. Res. Lett.*, *30*(15), 1801, doi:10.1029/2003GL017452.

Vidale, J. E., W. L. Ellsworth, A. Cole, and C. Marone (1994), Variations in rupture process with recurrence interval in a repeated small earthquake, *Nature*, *368*, 624–626.

Waldhauser, F., and W. L. Ellsworth (2000), A double-difference earthquake location algorithm: Method and application to the northern Hayward Fault, California, *Bull. Seismol. Soc. Am.*, *90*, 1353–1368.

Yu, S. B., and L. C. Kuo (2001), Present-day crustal motion along the Longitudinal Valley Fault, eastern Taiwan, *Tectonophysics*, *333*, 199–217.

Yu, S. B., H. Y. Chen, and L. C. Kuo (1997), Velocity field of GPS stations in the Taiwan area, *Tectonophysics*, *274*, 41–59.

K. H. Chen, K.-E. Ching, and R.-J. Rau, Department of Earth Sciences, National Cheng Kung University, 1 University Road, Tainan 701, Taiwan. (raurj@mail.ncku.edu.tw)